Inorganic Chemistry

pubs.acs.org/IC

Article

A Family of Lanthanide Hydroxo Carboxylates with 1D Polymeric Topology and Ln_4 Butterfly Core Exhibits Switchable Supramolecular Arrangement

Dimitry Grebenyuk, Mirijam Zobel, Maurizio Polentarutti, Liviu Ungur, Mikhail Kendin, Konstantin Zakharov, Pavel Degtyarenko, Alexander Vasiliev, and Dmitry Tsymbarenko*

Cite This: *Inorg. Chem.* 2021, 60, 8049–8061

Read Online

ACCESS | Metrics & More | Article Recommendations | Supporting Information

ABSTRACT: The unique family of coordination polymers $[Ln_4(OH)_2(piv)_{10}(H_2O)_2]_\infty$ of 11 lanthanides (Ln = La–Er) has been prepared by a simple solution method based on controlled hydrolysis. The ribbon-like polymeric structure consisting of connected tetranuclear clusters and supported by pivalate ligands and a framework of H-bonds has been revealed by single-crystal X-ray diffraction. While the compounds demonstrate similar PXRD patterns and unit cell parameters, the joint single-crystal XRD and pair distribution function data suggest the significant local structure change along the lanthanide series. The compounds exist as two packing polymorphs (α and β) with similar ribbon geometry, but different supramolecular arrangement of the ribbons. Dehydration of either polymorph does not disturb the tetranuclear core but leads to a translational symmetry loss along the ribbon and a transformation of the 3D-ordered crystal into a 2D-ordered mesostructure. Rehydration of the mesostructure leads to the β polymorph (except La and Ce), allowing the deliberate switching between the polymorphs via dehydration–rehydration evidenced by means of powder X-ray diffraction, pair distribution function analysis, and density functional theory calculations. Ab initio calculations reveal significant magnetic anisotropy of Ln^{3+} ions with ferro- and antiferromagnetic interactions within tetranuclear $[Ln_4(OH)_2(piv)_{10}(H_2O)_2]$ species. Magnetic susceptibility measurements demonstrated antiferromagnetic coupling, slow magnetic relaxation for Dy, Ho, and Er complexes, and field-induced single-chain magnetism for the Dy compound.

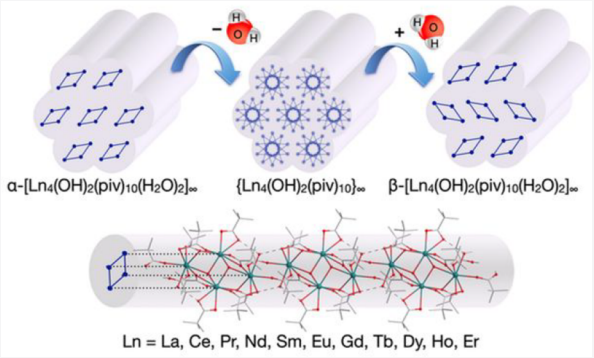

1. INTRODUCTION

Polynuclear coordination compounds of lanthanides have drawn significant attention due to their potential applications as magnetic,[1,2] luminescent,[3,4] bioactive,[5] and catalytic materials[6,7] and fascinating crystal structures. The similarity of chemical and structural properties of lanthanides allows one to finely control physical properties of the synthesized compounds by choice of a certain rare earth element. In particular, Gd-, Dy-, Ho-, and Er-based cluster compounds attract attention as molecular magnets with a large spin ground state and large magnetic anisotropy with potential applications in quantum computing,[8] high-density memory devices,[9] and magnetocaloric materials.[10−12] One of the most attractive architectures for these applications is a planar tetranuclear "butterfly" core.[2,13−19]

Although a variety of architectures from simple di- and trinuclear complexes to extremely complex ones containing up to 76 metal atoms per molecule[20] were reported to date, only two different synthetic approaches prevail to obtain a cluster compound. The first one is based on the careful hydrolysis of lanthanide nitrates, yielding $\{Ln_6(\mu_3\text{-}OH)_8\}$-based molecular clusters.[21,22] The second one is the controlled hydrolysis of a lanthanide salt in the presence of an organic ligand acting as a shield for the emerging polynuclear core and preventing it from further condensation into lanthanide hydroxide. This approach was found to be extremely versatile due to the variety of organic ligands available to control the hydrolysis: amino acids,[23] Schiff bases,[24,25] and diketones.[26−28] Recently, a novel two-step approach based on controlled hydrolysis and reconstruction of a hexanuclear $\{Ln_6(\mu_3\text{-}OH)_8\}$ core for the synthesis of the lanthanide hydroxo pivalate molecular clusters has been reported.[29]

In recent years, attempts have been made to use discrete molecular clusters of lanthanides as secondary building units to be joined into coordination polymers of different dimensionalities.[30,31] Those compounds attract a great deal of attention

Received: February 26, 2021
Published: May 18, 2021

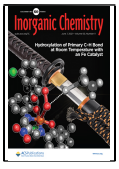

Scheme 1. Different Methods Applied for Synthesis and Respective Products for Each Ln[a]

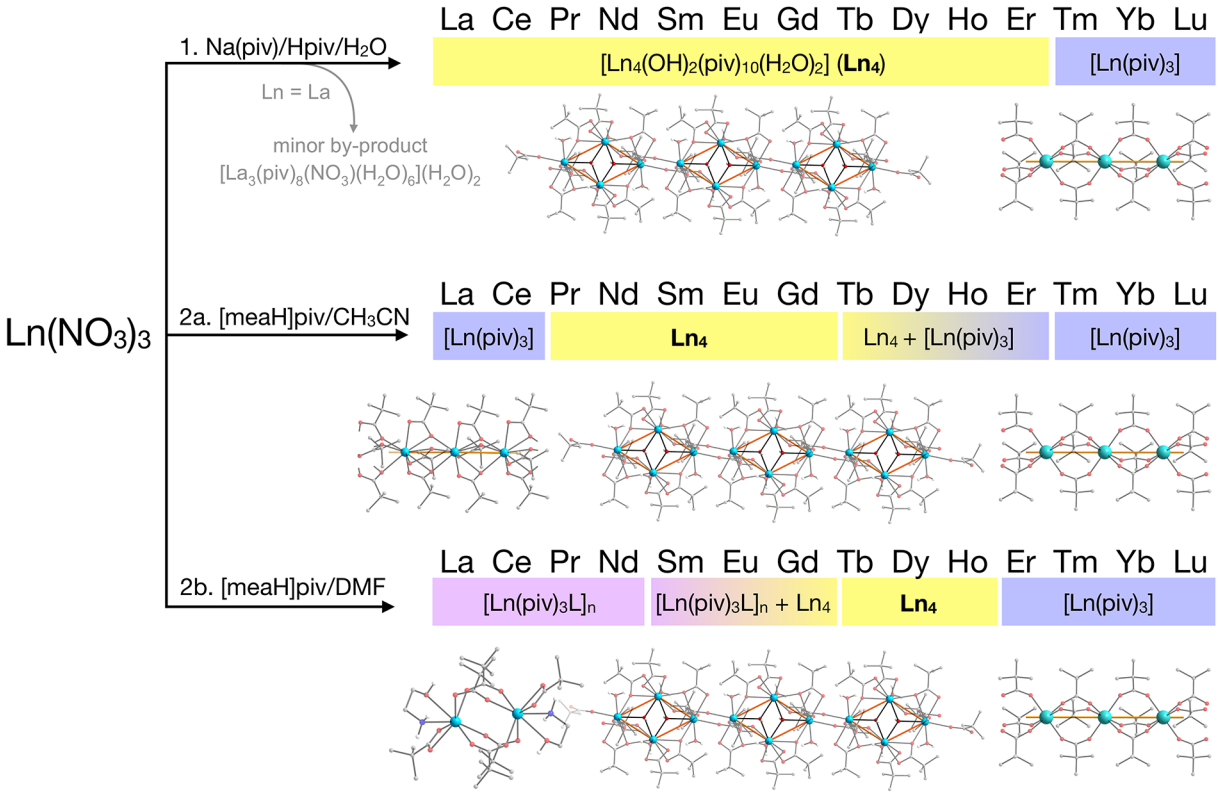

[a]The colored bars represent products with a particular composition. Note the overlapping regions in the case of non-aqueous solutions indicating a mixture of products. $[Ln(piv)_3L]_n$ is the general representation of mixed-ligand lanthanide pivalate complexes with monoethanolamine which were reported elsewhere.[49]

due to the variety of their possible applications as porous materials for gas sorption and separation,[32,33] selective catalysis,[7] sensing,[34−36] or drug delivery.[37] As the deliberate design and construction of coordination polymers from discrete preorganized polynuclear clusters of lower nuclearity, such as Ln_6 and Ln_4, is still a challenge, focusing on the chemistry of those clusters is the key to establishing new synthetic approaches and revealing the peculiarities of lanthanide interactions within a cluster.

A variety of tetranuclear lanthanide compounds have been characterized to date, defining the two most common architectures. The first one is a "cubane" $\{Ln_4(\mu_3\text{-}OH)_4\}$ core with a tetrahedral arrangement of metal atoms, frequently found both as a base of tetranuclear molecular compounds[38,39] and as a building block of more complex polynuclear structures made of several joint cubanes,[40,41] but also observed as building units of coordination polymers.[42−44] The second common tetranuclear cluster architecture is a $\{Ln_4(\mu_3\text{-}OH)_2\}$ or $\{Ln_4(\mu_3\text{-}O)_2\}$ butterfly core with a planar arrangement of four metal atoms. It has been often reported in different molecular complexes[2,13−19] as well as in coordination polymers.[45−47] Among them, the study of 1D coordination polymers with only a few inter-cluster connections may help to reveal how the linking of clusters would influence the intra-cluster interactions, e.g., magnetic exchange. As reported earlier, the shielding effect of bulky pivalate ligands (Hpiv, pivalic acid, $C(CH_3)_3COOH$) allows stabilizing both 1D coordination polymers[48] and polynuclear lanthanide clusters.[2]

Here, we report on the new family of 1D lanthanide hydroxo pivalates with a tetranuclear butterfly core for 11 lanthanides, the controlled transformation of their supramolecular organization, and their magnetic properties.

2. RESULTS AND DISCUSSION

Synthesis. Preparation of lanthanide hydroxo pivalates $[Ln_4(OH)_2(piv)_{10}(H_2O)_n]$ (**Ln$_4$**, Ln = La, n = 4; Ln = Ce−Er, n = 2) was performed by self-regulated hydrolysis via the reaction between lanthanide nitrates as a metal source and several aqueous (method 1) and nonaqueous (methods 2a and 2b) buffer media (Scheme 1). According to powder XRD data, as-obtained **Ln$_4$** compounds belong to the triclinic α-**Ln$_4$** structural type with a minor admixture of monoclinic β-**Ln$_4$** phase in some cases. Among the tested procedures, the equimolar aqueous solution of Na(piv) and Hpiv (pK_a (Hpiv) = 5.03) demonstrated higher reproducibility and yields. See Table S1 for the characterization data of the compounds.

During the adjustment of the method 1, we have obtained a trinuclear complex $[La_3(piv)_8(NO_3)(H_2O)_6](H_2O)_2$ as a minor byproduct (Scheme 1). We managed to isolate several single crystals of the compound and to determine its crystal structure (Figure S1; Tables S2, S3).

In general, two other reaction products—tris-pivalates $[Ln(piv)_3]_n$ and mixed-ligand complexes $[Ln(piv)_3L]_n$—can be formed in this system. For the beginning of the series, the preference toward higher coordination numbers often leads to a formation of mixed-ligand complexes with a saturated coordination environment.[49] Lanthanide contraction results

https://doi.org/10.1021/acs.inorgchem.1c00581
Inorg. Chem. 2021, 60, 8049−8061

in the decrease of coordination number, manifested, for instance, in the similar system of lanthanide tris-acetates.[50−54] At the same time, a smaller ionic radius makes the heavier lanthanides prone to hydrolysis, yielding hydroxo pivalates. For the smallest lanthanides (Tm, Yb, Lu), the shielding effect of bulky pivalate anions defines the formation of tris-pivalates without hydrolysis.[48]

Remarkably, both methods 1 and 2 lead to the products with an equal degree of hydrolysis, giving the evidence of high stability of the **Ln$_4$** architecture. At the same time, water as a solvent promotes hydrolysis, making the formation of hydroxo pivalates favorable for the widest range of lanthanides. Additionally, the hydrophobic nature of the pivalate ligand obstructs further condensation by shielding the polar lanthanide-oxygen cores, thus preventing deeper hydrolysis. The stability of the polynuclear architecture is confirmed by the results of MALDI MS (Figure S2).

Several synthetic procedures for the tetranuclear compounds containing a planar $\{Ln_4(\mu_3\text{-}OH)_2\}$ core supported by pivalate anions have been reported to date. The majority of them use triethylamine as a noncoordinating base to induce hydrolysis, and bulky capping agents (Schiff bases,[24,25] diketones,[26−28] triazole derivatives,[43] and phenol derivatives[55,56]) to prevent further hydrolysis. Abbas and co-workers[2] used *N*-methyldiethanolamine as a bifunctional ligand which acts as a base to support the hydrolysis and is at the same time coordinated to the metal cluster, preventing the process from proceeding deeper.

Method 1 here presented, in contrast to those mentioned above, does not require any additional base, since the hydrolysis is induced by the Hpiv/Na(piv) mixture itself. The intrinsic buffer properties of the mixture ensure a controlled hydrolysis by pH retaining. This feature of the method allows obtaining, in a reproducible way, pre-hydrolyzed **Ln$_4$** species to be used as precursors for other families of polynuclear compounds.[29]

The **Ln$_4$** compounds (either α or β) release water upon heating up to 200 °C in air and in argon, and up to 130 °C under vacuum (Figure S3), yielding dehydrated lanthanide species (hereafter referred to as **Ln$_4$′**) with few Bragg peaks on PXRD patterns. Deliberately soaking in water or long exposure of **Ln$_4$′** in air leads to their rehydration to **Ln$_4$** with the same water content measured for the as-obtained **Ln$_4$** according to IR, TG-DTA as well as PXRD data. The obtained polymorph after rehydration depends on the lanthanide: α-**Ln$_4$** for Ln = La, Ce and β-**Ln$_4$** for Ln = Pr−Er (Figure S4). The structures of the crystalline **Ln$_4$** species and the details of structural transformations during dehydration and rehydration are discussed further below, with the support of XRD, pair distribution function (PDF), and DFT data.

X-ray Crystal Structures. The **Ln$_4$** crystal structures appeared in two polymorphic forms—a triclinic one (referred to as α-**Ln$_4$**) and a monoclinic one (β-**Ln$_4$**). Both polymorphs contain 1D $[Ln_4(OH)_2(piv)_{10}(H_2O)_2]_\infty$ ribbons of similar geometry, noticeably differing in the packing motif of the ribbons within the structure.

Crystal Structure of α-Ln$_4$. The triclinic α-**Ln$_4$** polymorph has been observed for Ln = La−Er at both low and room temperature (Table S4). Three subtypes of this polymorph exist: $[La_4(OH)_2(piv)_{10}(H_2O)_4]$ (α-**La$_4$**, Figure S5); $[Ln_4(OH)_2(piv)_{10}(H_2O)_2]$, Ln = Ce−Dy ($\alpha$-**Ce$_4$**); $[Ln_4(OH)_2(piv)_{10}(H_2O)_2]$, Ln = Ho, Er ($\alpha$-**Er$_4$**, Figure S6). As the second one is the most common subtype, the structure of α-**Ce$_4$** is described here in detail. The difference between the subtypes will be discussed further below. The refinement data can be found in Table S5.

The triclinic unit cell of α-**Ce$_4$** contains centrosymmetric tetranuclear species $\{Ln_4(OH)_2(piv)_{10}(H_2O)_2\}$ with a "butterfly" $\{Ln_4(\mu_3\text{-}OH)_2\}$ core considered as a building unit of the 1D ribbon (Figure 1). Two crystallographically independent Ln^{3+} ions, labeled as Ln1 and Ln2 both with coordination numbers of 8, exhibit different coordination environments.

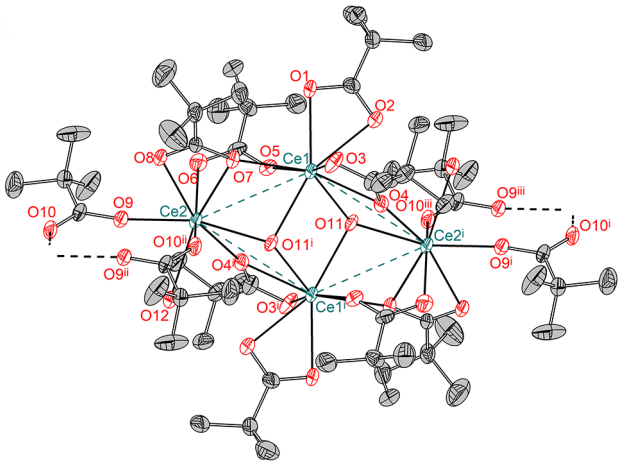

Figure 1. Tetranuclear fragment $[Ce_4(OH)_2(piv)_{10}(H_2O)_2]$ in the α-**Ce$_4$** structure. Symmetry codes: (i) $1-x, 1-y, 2-z$; (ii) $2-x, 1-y, 2-z$; (iii) $1-x, y, z$. Dashed lines connecting Ce atoms highlight the planar tetranuclear $\{Ln_4(\mu_3\text{-}OH)_2\}$ core.

Ln1 is coordinated by O1 and O2 atoms of a κ^2-carboxylate group, O3 and O4 atoms of a μ_2-κ^1:κ^2-carboxylate group, O7 atom of a second μ_2-κ^1:κ^2-carboxylate group, O5 atom of a μ_2-κ^1:κ^1-carboxylate group, and O11, O11^i atoms of two μ_3-OH groups. Ln2 is coordinated by O6 atom of a μ_2-κ^1:κ^1-carboxylate group, O7 and O8 atoms of a μ_2-κ^1:κ^2-carboxylate group, one O11 atom of a μ_3-OH group, O12 atom of a water molecule, and O9, O10^{ii} atoms of two μ_2-κ^1:κ^1-carboxylate groups which bridge the tetranuclear core to the neighboring one. Each metal is thus coordinated by five pivalate anions exhibiting different coordination modes. Coordination polyhedra of the Ln atoms were determined using the continuous shape measures (CShM) approach implemented in SHAPE2.1 software[57] (Tables S6−S9, Figure S7). The full list of Ln···O interatomic distances and H-bond parameters can be found in Tables S10 and S11, respectively.

The distances between the three closest Ln atoms within a tetranuclear core of any **Ln$_4$** are ranging from 3.7 to 4.2 Å (Figure 2, Table S12), with the smallest Ln···Ln distance between neighboring cores being ca. 5.0 Å. Along the lanthanide series, the Ln1···Ln2 and Ln1···Ln1^i distances gradually decrease together with ionic radius, whereas the Ln1···Ln2^i distance has a minimum. A steep increase of the distance for smaller lanthanides (Tb−Er) indicates the significant steric hindrances. Those are the reasons why the hydroxo pivalates have not been detected for the smallest lanthanides (Tm, Yb, Lu).

Despite the stability of the tetranuclear $\{Ln_4(\mu_3\text{-}OH)_2\}$ core for lanthanides from La to Er, lanthanide contraction leads to the evolution of the structure along the lanthanide series, resulting in formation of three distinct subtypes of the α-**Ln$_4$**

https://doi.org/10.1021/acs.inorgchem.1c00581
Inorg. Chem. 2021, 60, 8049−8061

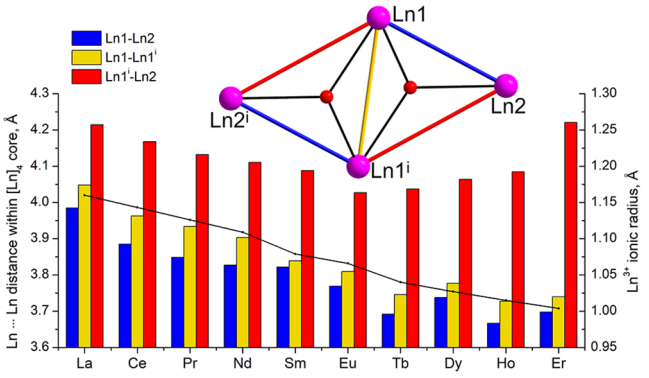

Figure 2. Ln···Ln distances in the $\{Ln_4(\mu_3\text{-}OH)_2\}$ core. Symmetry code: (i) $1-x, 1-y, 2-z$. The markers connected with the black line indicate the ionic radius of a particular lanthanide.

crystal structure. The crystal structure of α-**La$_4$** (Figures S5, 3a) differs from the one of α-**Ce$_4$** in the extra water molecule (O13) coordinating La1, which acquires the coordination number of 9, while structural functions of the pivalate ligands are the same as in α-**Ce$_4$** with similar Ln−O distances (Table S10). In the crystal structure of α-**Er$_4$**, (Figures S6, 3a), one of the pivalate ligands (O3, O4) has a μ_2-κ^1:κ^1 coordination mode instead of μ_2-κ^1:κ^2 in α-**Ce$_4$**, resulting in the coordination number of 7 for the Er1 atom.

Noticeably, the difference between the three α-**Ln$_4$** subtypes with significant variation of the local structure is not manifested in the PXRD patterns of the compounds (Figure 3b). Therefore, the technique sensitive to the local structure is required to support the findings of single-crystal XRD analysis. The PDF data were collected for α-**La$_4$**, α-**Ce$_4$**, and α-**Er$_4$** and refined using the structural models obtained from the single-crystal XRD analysis (Figure 3c). The experimental data are well described by the models, including the noticeable change in the region of 3−5 Å originating from the transformation of the lanthanide-oxygen core local structure (Figure 3a). Additional PDF refinements performed for the α-**La$_4$**, α-**Ce$_4$**, and α-**Er$_4$** experimental data with only the α-**La$_4$** model produced significantly poorer results (Figure S8), also supporting the initial findings.

The shielding effect of hydrophobic pivalate anions and slight transformations of the local structure stabilize the 1D polymeric structure of **Ln$_4$** for almost the whole row of lanthanides. Additional stabilization arises from the H-bond network formed by the coordinated water molecules and pivalate anions (Table S11). The μ_3-OH anion seems not to be involved into formation of H-bonds, as the shortest distance of 2.684 Å between O11···O10^{iii} atoms corresponds to an unreliable O−H···O angle of ca. 104° for α-**Ce$_4$**.

Within the crystal structure, **Ln$_4$** ribbons are packed along the crystallographic direction *a*, and their lanthanide atoms are projected onto an oblate rhombus in the *bc* plane (Figure 4a,b). The Ln1 and Ln2 ions with their symmetry-related equivalents from neighboring tetranuclear clusters define two distinct planes (green and purple, respectively, Figures 4, S9) with 78° of mutual inclination. In this view, for the α polymorph, the ribbons are packed in the one-layered manner with the projections of those planes being parallel to each other (Figure 4c, S10) with a clearly visible 2D pseudo-hexagonal motif. The respective 2D lattice parameters *u* and *v* are almost equal to each other, and the φ angle between them is close to 120° (Table S4).

Crystal Structure of β-Ln$_4$. The monoclinic unit cell of the β-**Ln$_4$** polymorph contains centrosymmetric tetranuclear species $\{Ln_4(OH)_2(piv)_{10}(H_2O)_2\}$ with a "butterfly" $\{Ln_4(\mu_3\text{-}$

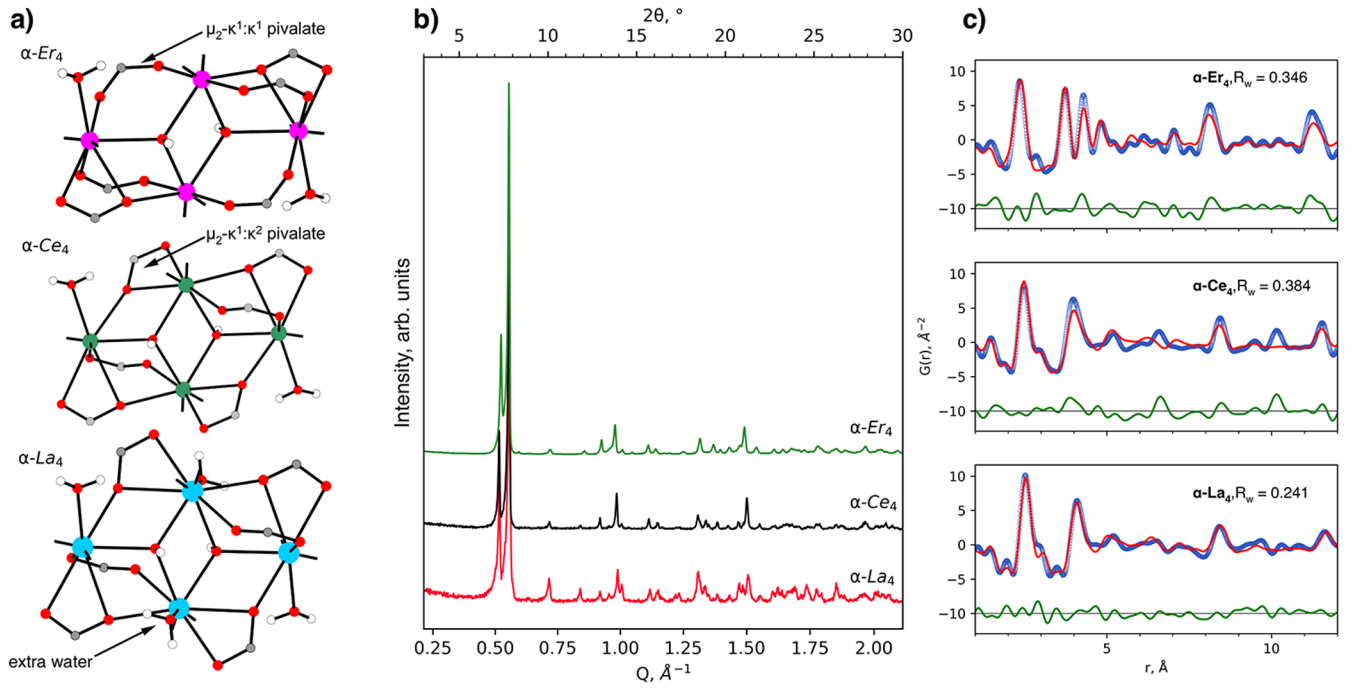

Figure 3. (a) Lanthanide-oxygen cores of the three subtypes of α-**Ln$_4$**, according to the single-crystal X-ray analysis. (b) PXRD patterns of as-obtained **Ln$_4$** (Ln = La, Ce, Er) compounds belonging to three α-**Ln$_4$** subtypes, λ = 1.5406 Å. *Q* is the modulus of a scattering vector transfer, $Q = 4\pi \sin\theta/\lambda$. (c) PDF fits (red solid line) of measured data (circles) with the corresponding α-**Ln$_4$** hydroxo pivalate models from the single-crystal X-ray analysis for the distance range 1−12 Å. Difference curves are offset for clarity.

https://doi.org/10.1021/acs.inorgchem.1c00581
Inorg. Chem. 2021, 60, 8049−8061

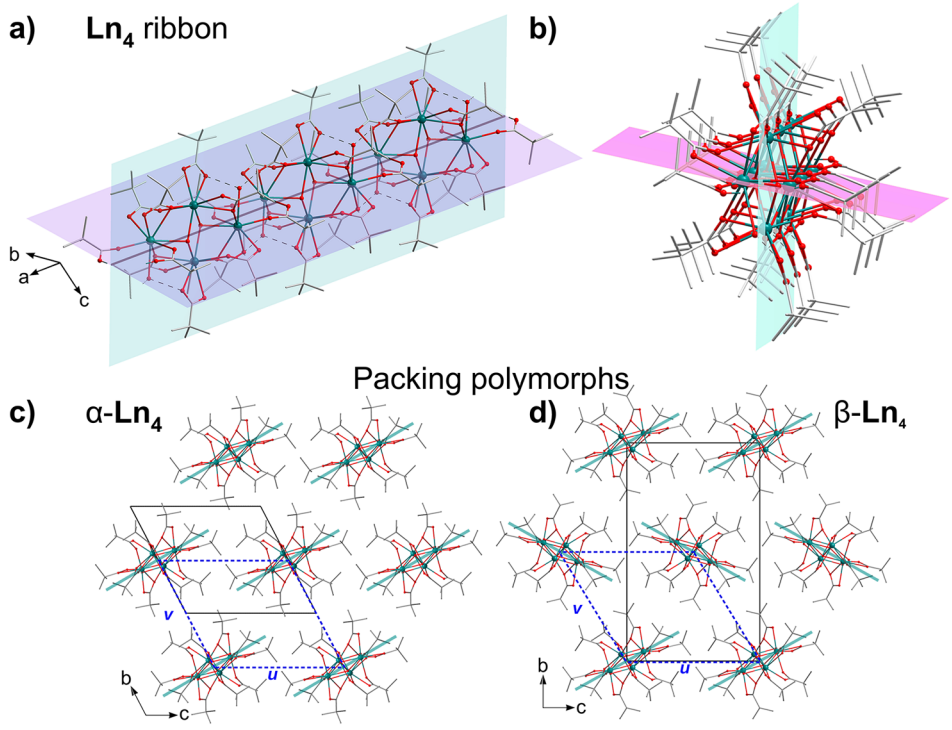

Figure 4. (a) Arrangement of $\{Ln_4(\mu_3\text{-}OH)_2\}$ cores into 1D $[Ln_4(OH)_2(piv)_{10}(H_2O)_2]_\infty$ polymeric ribbon in the crystal structure of α-**Ce$_4$**. The dashed lines represent O−H···O bonds between water molecules and pivalate anions. Ln1 and Ln2 planes are highlighted. (b) View of the $[Ln_4(OH)_2(piv)_{10}(H_2O)_2]_\infty$ ribbon along the direction *a*. (c) Triclinic α packing polymorph of $[Ln_4(OH)_2(piv)_{10}(H_2O)_2]_\infty$. (d) Monoclinic β packing polymorph of $[Ln_4(OH)_2(piv)_{10}(H_2O)_2]_\infty$. H atoms are omitted for clarity. Black lines show unit cell edges. Difference in packing is highlighted by pale green lines. Dashed blue lines show pseudo-hexagonal 2D lattice based on *u* and *v* basis vectors.

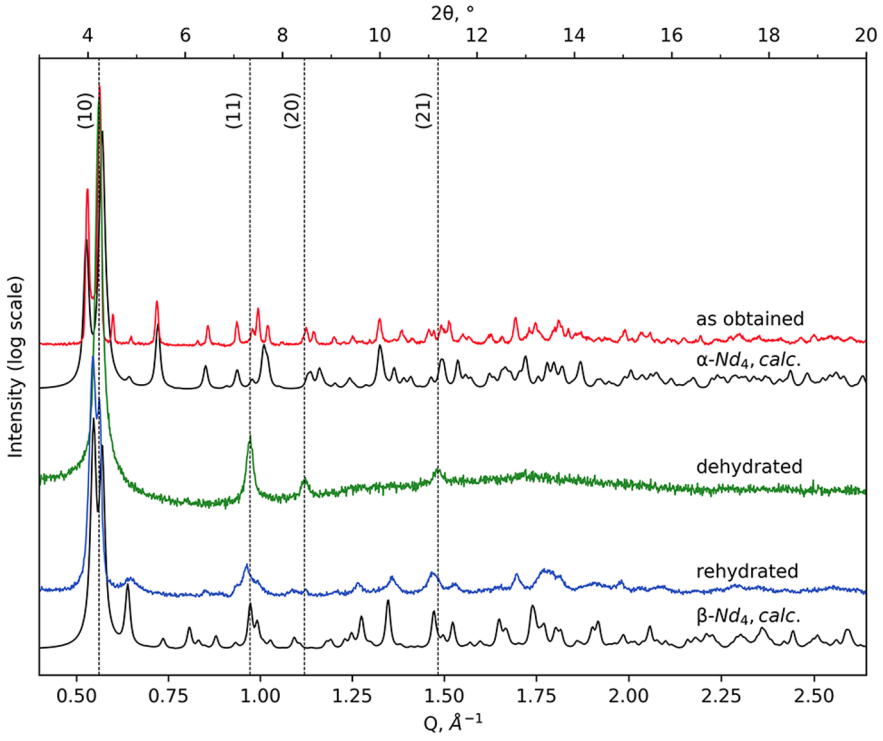

Figure 5. PXRD patterns of as-obtained **Ln$_4$**, dehydrated **Ln$_4$′**, and rehydrated **Ln$_4$** compounds for Ln = Er. Calculated PXRD patterns for α-**Nd$_4$** and β-**Nd$_4$** are given for reference. Vertical dashed lines show calculated peak position and 2D Bravais hexagonal lattice indices with lattice parameters $u = v = 12.95$ Å. $\lambda = 0.8266$ Å.

https://doi.org/10.1021/acs.inorgchem.1c00581
Inorg. Chem. 2021, 60, 8049−8061

$OH)_2$} core. Two crystallographically independent eight-fold coordinated Ln1 and Ln2 ions show coordination environments similar to those of the α-$\mathbf{Ln_4}$ structure, and differences between corresponding Nd−O distances in α-$\mathbf{Nd_4}$ and β-$\mathbf{Nd_4}$ do not exceed 0.03 Å (Table S10). In contrast to α-$\mathbf{Ln_4}$, ribbons in β-$\mathbf{Ln_4}$ form two-layered packing in the *bc* plane with the *bc* projections of neighboring layers twisted by 58° (Figure 4d).

Although the tetranuclear "butterfly" building unit is frequently present in lanthanide compounds as a core of isolated molecular entities,[2,13−19] to the best of our knowledge, only few coordination polymers constituted of connected butterfly clusters have been reported to date.[45,46] Abbas and co-workers[2] have reported the family of $[Ln_4(OH)_2(mdeaH)_2(piv)_8]$ (Ln = Tb−Tm) molecular compounds isolated from a system of lanthanide nitrate, pivalic acid, and *N*-methyldiethanolamine ($mdeaH_2$). The latter acted both as a base (promoting lanthanide hydrolysis) and as a capping ligand providing the molecular structure of the obtained cluster compounds. According to continuous shape measures (CShM) analysis (Tables S6−S9), the arrangement of ligands within the coordination sphere of $[Ln_4(OH)_2(mdeaH)_2(piv)_8]$ is close to that of $[Ln_4(OH)_2(piv)_{10}(H_2O)_2]_\infty$. Both families include magnetically active lanthanides Dy, Ho, and Er which allows specifying the effect of the "butterfly" cluster joining on magnetic properties of the compounds.

Switching of Supramolecular Arrangement by Dehydration−Rehydration. According to powder XRD data, as-obtained $\mathbf{Ln_4}$ compounds (Ln = La−Er) belong to the triclinic α-$\mathbf{Ln_4}$ structural type with a minor admixture of the monoclinic β-$\mathbf{Ln_4}$ phase in some cases. The intense Bragg peaks at small angles (3.5−4.5° for λ = 0.8266 Å) in the XRD patterns (Figure 5) correspond to (001), (0−11), and (010) planes (Figure S10). All of these planes with slightly different interplanar distances originate from a pseudo-hexagonal close packing of 1D ribbons (Figure 4) with u = 12.5 Å, v = 13.5 Å, φ = 118° for α-$\mathbf{Nd_4}$.

Heat treatment of α-$\mathbf{Ln_4}$ powder, under either air or vacuum conditions, leads to elimination of coordinated water molecules and to a solid-state transformation to an anhydrous $\mathbf{Ln_4}'$ compound ($[Ln_4(OH)_2(piv)_{10}]_\infty$) showing a reduced-order mesostructure. The XRD pattern of $\mathbf{Ln_4}'$ contains only a few Bragg peaks which are perfectly indexed as a hexagonal 2D Bravais lattice with lattice parameters for $\mathbf{Nd_4}'$ $u = v$ = 13.074 Å, φ = 120°, corresponding to a hexagonal supramolecular arrangement of cylindrical ribbons, while there are no Bragg peaks that would indicate translation symmetry along the ribbon.

It is worth noting that rehydration results in 2D lattice parameters u, v, φ in the β-$\mathbf{Ln_4}$ phase, which deviate less from the ideal hexagonal values than in the α-$\mathbf{Ln_4}$ phase (Table S4). In this view, although the transition of $\mathbf{Ln_4}'$ to β-$\mathbf{Ln_4}$ (and not to α-$\mathbf{Ln_4}$) should be preferable, the DFT calculations do not report any remarkable difference in total lattice energies of the two packing polymorphs (see Quantum chemical calculations in the Supporting Information (SI)).

Although PXRD can elucidate the switching between different packing of the $\mathbf{Ln_4}$ ribbons, no information on intra-ribbon transformations can be extracted from Bragg scattering data. In order to gain information on the local structure, total X-ray scattering experiments with PDF analysis supported by DFT modeling have been performed.

PDF Study of Local Structure Evolution. As described above, the intense low-angle Bragg peaks (at Q = 0.55 $Å^{-1}$) in PXRD patterns of as-obtained α-$\mathbf{Ln_4}$, dehydrated $\mathbf{Ln_4}'$, and rehydrated β-$\mathbf{Ln_4}$ correspond to pseudo-hexagonal packing of 1D ribbons in the *bc* plane (Figure S10). In order to extract the information on the intra-ribbon structure and its evolution, these peaks have been omitted for PDF calculation and refinement as they only contain information on this packing mesostructure (Figure S11), using an approach already employed for the study of metal−organic frameworks and metal oxide nanoparticles.[58,59] Its validity for the $\mathbf{Ln_4}$ system is further reasoned in the SI.

The PDF data were collected, and the refinements were performed for triclinic α-$\mathbf{Sm_4}$, 2D-mesostructured $\mathbf{Sm_4}'$, and monoclinic β-$\mathbf{Sm_4}$. Local structures of as-obtained α-$\mathbf{Sm_4}$ (Figure 6a) and rehydrated β-$\mathbf{Sm_4}$ (Figure 6c) proved to be

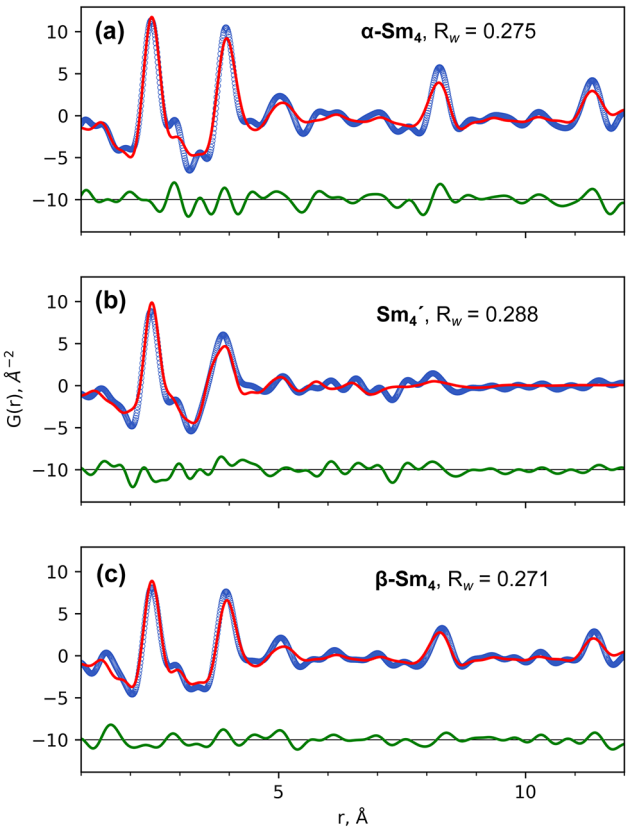

Figure 6. PDF fits (red solid line) of measured data (circles) with the Sm hydroxo pivalate models for the distance range 1−12 Å: (a) triclinic α-$\mathbf{Sm_4}$ phase (as obtained) fitted with 1D ribbon model (Figure S12a); (b) 2D-mesostrucured $\mathbf{Sm_4}'$ phase (dehydrated) fitted with $Sm_4(OH)_2(piv)_{10}$ 0D cluster model (Figure S12c); (c) monoclinic β-$\mathbf{Sm_4}$ phase (rehydrated) fitted with 1D ribbon model. Difference curves are offset for clarity. See Figure S13 for a PDF on a distance range up to 40 Å.

similar to each other and in agreement with results of SC XRD of $\mathbf{Ln_4}$. In particular, the most intense peaks in the experimental PDFs fit well with Sm···O (2.5 Å) and Sm···Sm (4.0 Å, 8.1 Å, 11.3 Å) interatomic distances.

For the PDF refinements of both crystalline $\mathbf{Sm_4}$ samples, α-$\mathbf{Sm_4}$ and β-$\mathbf{Sm_4}$, a single isolated 1D ribbon-like supramolecule (of ca. 80 Å length) has been set up from the room

https://doi.org/10.1021/acs.inorgchem.1c00581
Inorg. Chem. 2021, 60, 8049−8061

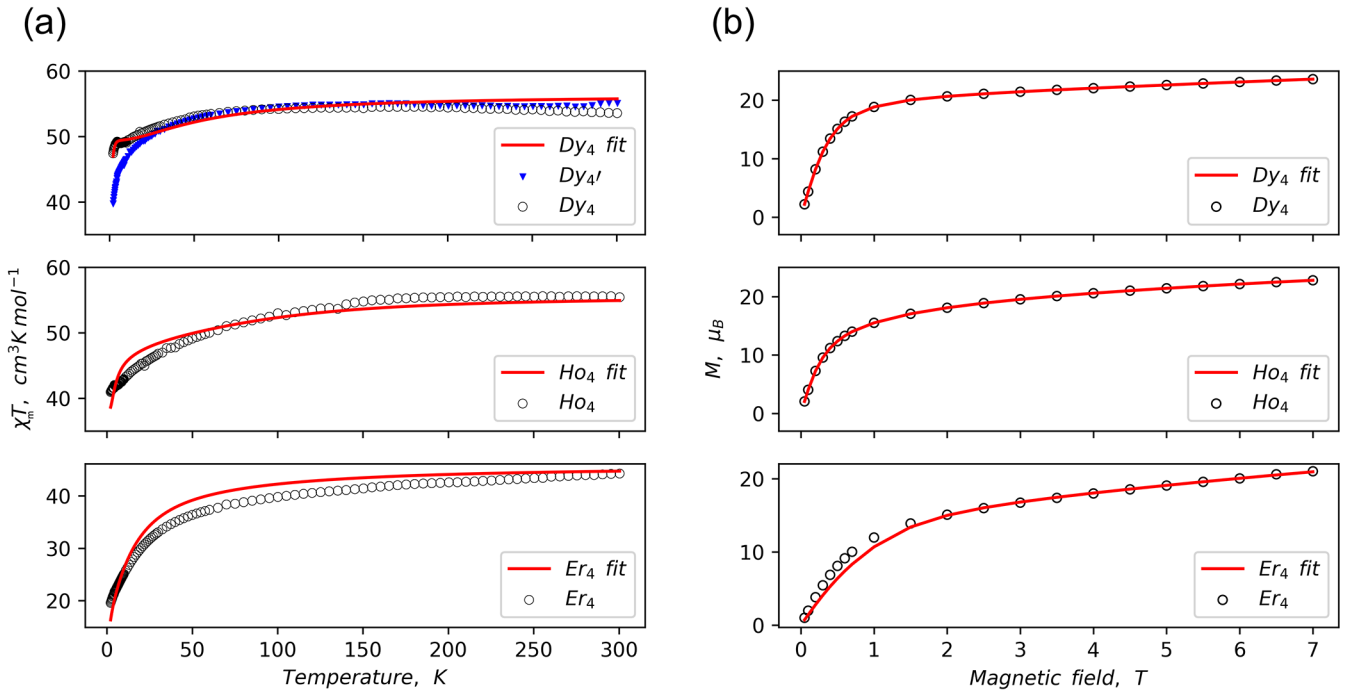

Figure 7. Magnetic properties of as obtained **Dy$_4$**, **Ho$_4$**, **Er$_4$**, and dehydrated **Dy$_4$′** compounds: (a) Temperature dependence of $\chi_m T$ product at 1000 Oe; (b) magnetization versus applied field at 2 K. Symbols show measured data; solid lines are the theoretical fits using the POLY_ANISO routine.

temperature DFT relaxed crystal structure of β-**Sm$_4$** and applied as a structural model (Figure S12, Table S13).

The experimental data are well described by this model, without further refinement of its structural parameters (atomic coordinates and atomic displacement parameters).

The PDF of the dehydrated 2D-mesostructured **Sm$_4$′** (Figure 6b) reveals that the local structures in the dehydrated and crystalline compounds are similar in terms of the closest Sm···O (2.5 Å) and Sm···Sm (4.0 Å) distances. For a longer range, the structures (and hence PDFs) differ. In the dehydrated **Sm$_4$′**, the peaks at 8.1 and 11.3 Å are absent, corresponding to Sm···Sm distances from atoms in neighboring tetranuclear clusters in the hydrated phases. The 11.3 Å peak is a translation vector along the ribbon (which is aligned with crystallographic axis *a*). The experimental data are well described by the DFT-optimized model of the molecular $Sm_4(OH)_2(piv)_{10}$ cluster (Figure S12) which has the same local structure as **Sm$_4$** (confirming the integrity of the cluster), but no translational symmetry, supporting the thesis of reversible disordering−ordering of tetranuclear clusters along the ribbon upon dehydration−rehydration.

Magnetic Study. The Ln_4 clusters with a butterfly core have been actively studied for the past decade, and Ln_4 single molecule magnet (SMM) compounds with record blocking temperature have been reported.[60] The previous data highlight the pivotal role of the ligand field in the appearance of magnetic anisotropy for lanthanide ions. Although Shiff bases, beta-diketonates, pirazolates, and carboxylates (pivalates) were reported to be appropriate choices for the construction of Ln_4 clusters with slow magnetic relaxation,[14,16,55,61−64] no significant attention has been paid to date to the intermolecular arrangement of tetranuclear clusters, supposing magnetic behavior to be more strongly affected by the local coordination environment. The reported **Ln$_4$** compounds give the unique opportunity to reveal the effect of clusters connection and modification of the magnetic properties.

In order to unveil the influence of 1D ribbon topology and supramolecular arrangement on magnetic behavior in contrast to isolated molecular Ln_4 butterfly clusters, the polycrystalline powders of as-obtained **Dy$_4$**, **Ho$_4$**, and **Er$_4$** (α polymorphs) as well as a powder of dehydrated **Dy$_4$′** have been studied by direct-current and alternating-current magnetic measurements in the temperature range of 2−300 K.

The direct current (dc) magnetic data are summarized in Table S14. The room-temperature values of $\chi_m T$ (Figure 7a) are generally close to the expected values of four non-interacting Ln^{3+} ions (Table S14).

The temperature dependence of magnetic susceptibilities of **Dy$_4$**, **Ho$_4$**, **Er$_4$**, and **Dy$_4$′** compounds shows a similar behavior in terms of $\chi_m T$ product, which results to be almost temperature-independent in the range of 300−50 K and gradually decreases upon further cooling. This behavior is normally observed for other lanthanide clusters and can be attributed to thermal depopulation of Stark sublevels of Ln^{3+} ions, as well as to antiferromagnetic coupling.

Therefore, for purely qualitative comparison of magnetic behavior within the series, we have performed Curie−Weiss fits of higher temperature $\chi_m T$ data (Figures S14−S17) which showed the antiferromagnetic behavior of all compounds, but more pronounced for **Ho$_4$** and **Er$_4$**. It is worth noting that the $\chi_m T$ product of **Dy$_4$** shows a tangible kink in the lower temperature region with a maximum at 4.6 K, while **Dy$_4$′** demonstrates a faster decrease of $\chi_m T$ than **Dy$_4$** (the corresponding values of Weiss constant (θ) are equal to −1.63(8) and −0.72(11) K, respectively) without any anomalies. Thus, despite the almost identical local structure of **Dy$_4$** and **Dy$_4$′** compounds, the dehydration procedure affects the magnetic behavior. This effect can be ascribed to structural changes and relative shortening of the inter-cluster

https://doi.org/10.1021/acs.inorgchem.1c00581
Inorg. Chem. 2021, 60, 8049−8061

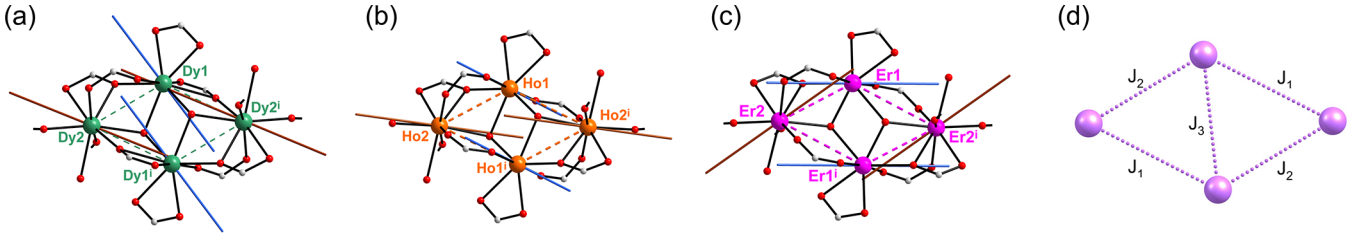

Figure 8. Schematic representation of the g tensor of each Ln center in $\{Dy_4(OH)_2(piv)_{10}(H_2O)_2\}$ (a), $\{Ho_4(OH)_2(piv)_{10}(H_2O)_2\}$ (b), and $\{Er_4(OH)_2(piv)_{10}(H_2O)_2\}$ (c). Exchange parameters within the tetranuclear core (d). Blue lines are for Ln1 and Ln1^i; brown lines are for Ln2 and Ln2^i. *tert*-Butyl groups of pivalate ligands are omitted for clarity.

distances and rearrangement of Dy ions' magnetic anisotropy axes.[62]

The isothermal magnetization of **Dy_4**, **Ho_4**, **Er_4**, and **Dy_4'** examined at 2 K gradually increases along with the applied dc field without saturation, even at 7 T (Figures 7b, S18, S19). The highest values of magnetization (Table S14) are considerably smaller than the values expected for four isolated Ln^{3+} ions. This behavior could indicate the existence of magnetic anisotropy and/or the presence of low-lying excited states.[65] Plots of magnetization−magnetic field response for all reported compounds at 2 K reveal the presence of a hysteresis effect with a very small coercive field (about 12 Oe) similarly to isolated **Dy_4** clusters at 1.8 K.[2]

To gain a deeper insight into the magnetic behavior of **Ln_4** polymers, the high-level ab initio CASSCF/RASSI-SO/SINGLE_ANISO calculations have been performed. The Ln1 and Ln2 ions within the Ln_4 cluster have noncollinear magnetic anisotropy axes (Figure 8). Table S16 shows calculated low-lying energy states as well as the g tensor of the ground doublet states on individual lanthanide states in the investigated compounds. The orientation of magnetic axes varies for a specific Ln; thus, for Dy_4, magnetic axes lie almost in the mean plane of the Ln_4 core, whereas Ho_4 and Er_4 are inclined to the plane by 21−56° and 11−14°, respectively (Table S15). The energy separation between the ground state and the first excited state is larger for Ln1 sites compared to Ln2 sites, for all investigated compounds (Figure 9 and Table S16). This is in line with stronger magnetic anisotropy in the ground state of sites Ln1 compared to sites Ln2. The DFT-optimized **Dy_4** structure follows in large the above trends.

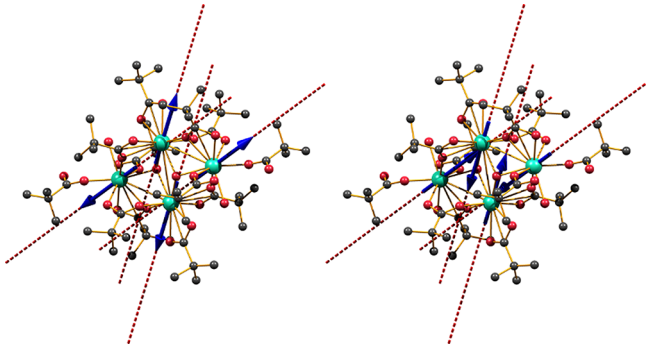

Figure 9. Local magnetic axes (g_Z, dashed lines) and of the local magnetic moments (blue arrows) in the two lowest exchange states in $\{Dy_4(OH)_2(piv)_{10}(H_2O)_2\}$ (marked bold in Table S17).

The magnetic interactions between Ln^{3+} ions include contributions from magnetic dipole−dipole and exchange interactions. The exchange coupling was simulated within the Lines model as described elsewhere.[66,67] Magnetic behavior of four interacting Ln^{3+} ions was described using the Lines exchange Hamiltonian (eq 1), with three coupling constants (Figure 8d)

$$\hat{H}_{exch} = -J_1(\hat{s}_1\hat{s}_{2i} + \hat{s}_{1i}\hat{s}_2) - J_2(\hat{s}_1\hat{s}_2 + \hat{s}_{1i}\hat{s}_{2i}) - J_3\hat{s}_1\hat{s}_{1i} \quad (1)$$

where s_i are projection operators of the effective spin of the Ln ion on the corresponding anisotropy axis (Figure 8d). J_i are the parameters of the inter-site magnetic exchange interaction and represent the only fitting parameters of the employed model. The inter-site magnetic dipole−dipole interaction is computed using eq 2 and added to the exchange Hamiltonian

$$\hat{H}_{dip}(i,j) = \mu_{Bohr}^2 \times \frac{\hat{\mu}_i\cdot\hat{\mu}_j - 3(\hat{\mu}_i\cdot n_{ij})(\hat{\mu}_j\cdot n_{ij})}{r_{ij}^3} \quad (2)$$

where $\hat{\mu}_i$ and $\hat{\mu}_j$ are the magnetic moments on the sites i and j, respectively, as obtained from the SINGLE_ANISO single-site calculations, n_{ij} is the normalized vector connecting sites i and j (of length = 1), r_{ij} is the distance between magnetic sites i and j, and μ_{Bohr}^2 is the square Bohr magneton constant, with an approximate value of 0.4329702 cm^{-1}/Tesla. The total Hamiltonian of magnetic interaction is a sum of the two operators:

$$\hat{H}_{total} = \hat{H}_{exch} + \hat{H}_{dip} \quad (3)$$

The low-lying energy spectra data obtained by diagonalization of the $\hat{H}_{total}$ and of individual $\hat{H}_{exch}$ and $\hat{H}_{dip}$ are given in Table S17. The energy splitting gives a rough estimation of the importance of exchange and dipolar couplings on the total interaction. As such, for **Dy_4**, the dipole−dipole interaction induces a stronger energy splitting compared to exchange interaction, whereas, in the case of **Ho_4** and **Er_4**, the exchange and dipolar interactions are of comparable strengths.

The eigenstates of $\hat{H}_{total}$ are further used for the description of magnetic susceptibility and molar magnetization of the entire tetranuclear compounds. The parameters J_i were found by minimization of the standard deviation function between measured and calculated magnetic susceptibility. Given that the exchange interaction is rather weak and induces weak splitting, only the low-temperature experimental data points, below 70 K, were considered in the fitting. This task was achieved within the POLY_ANISO code.[67]

Observed values of coupling parameters are close to those reported for the related molecular Ln compounds with a butterfly core. Moreover, the simulated $\chi_m T$ curve reproduces well the low temperature anomaly on the experimental data of the **Dy_4** compound, despite that the theoretical model included only a single **Ln_4** cluster. This proves that the anomaly indeed

https://doi.org/10.1021/acs.inorgchem.1c00581
Inorg. Chem. 2021, 60, 8049−8061

originates from the interplay between antiferro and ferro-intra-cluster magnetic interactions (see Table 1).

Table 1. Fitted Values of the Magnetic Exchange Interactions between Ln^{3+} Ions in Ln_4 (in cm^{-1})[a]

	J_1 (cm^{-1})	J_2 (cm^{-1})	J_3 (cm^{-1})
Dy_4	−0.0747	−0.0785	0.0900
Ho_4	−0.144	−0.168	0.442
Er_4	−0.460	−1.072	−0.703

[a]The dipole−dipole contribution was computed using the Hamiltonian in eq 2 and added to the exchange Hamiltonian. The relative energy splitting corresponding to various contributions to the magnetic interaction is given in Table S17.

Further experimental study of the magnetic behavior of **Dy_4**, **Ho_4**, **Er_4**, and **Dy_4'** has been performed by alternating current (ac) magnetic measurements in zero dc field within the temperature range of 2−10 K. Temperature dependence of out-of-phase (χ'') signals for **Dy_4**, **Dy_4'**, **Ho_4**, and **Er_4** shows a remarkable frequency dependence below 6 K which indicates the appearance of a slow magnetization relaxation phenomena. Assuming the relaxation of magnetization to be a Debye process, the energy barrier U_{eff} and relaxation time τ_0 were estimated using the approach described elsewhere (Figures S26−S29).[68] However, no expected maxima in out-of-phase ac susceptibility have been registered in a temperature range of 2−10 K even for Dy compounds without applying the external magnetic field (Figure 10). This behavior is common for lanthanide-based molecular magnets and presumably originates from the existence of a fast quantum tunneling relaxation of the magnetization (QTM) promoted by inter-cluster dipolar interactions.[69] In this view, the connection of isolated Dy_4 hydroxo pivalate clusters (which had demonstrated a maximum on χ'' at 2−3 K for 50−1000 Hz)[2] into the 1D coordination polymer leads to the enhancement of QTM effect and results in a shift of the possible maximum of χ'' toward temperatures below the examined range.

Noticeably, if an external magnetic field of 3000 Oe is applied to **Dy_4**, the QTM is suppressed and the maximum in χ'' appears at 3 K at frequencies higher than 3000 Hz, indicating a field-induced single-chain magnetism (Figure 11).

3. CONCLUSIONS

A new synthetic route based on controlled hydrolysis for a new family of polynuclear lanthanide hydroxo pivalate complexes has been developed. The complexes have been assembled via the connection of tetranuclear butterfly cores into a 1D

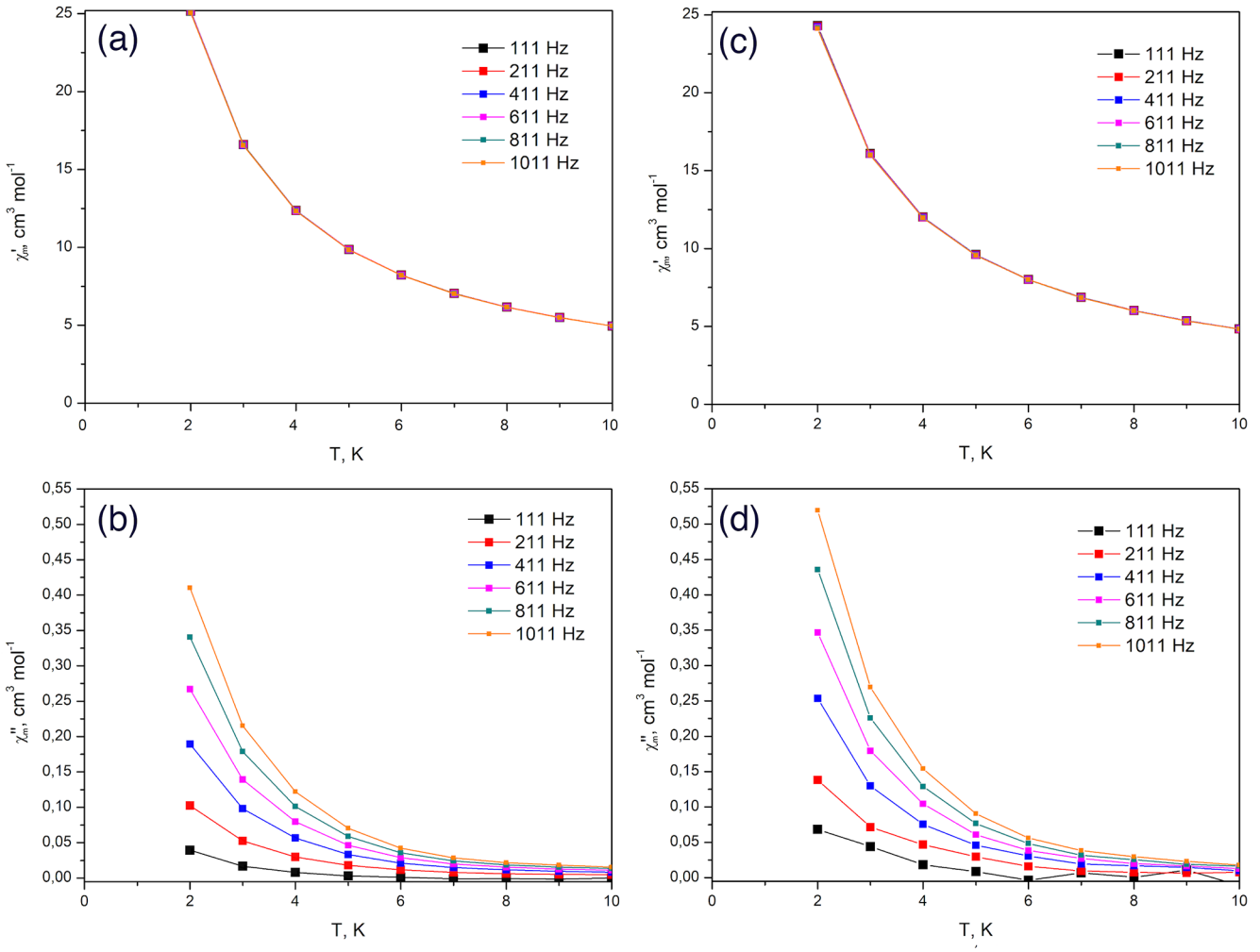

Figure 10. Temperature-dependent in-phase χ' and out-of-phase χ'' ac susceptibilities plots at different frequencies for **Dy_4** (a, b) and **Dy_4'** (c, d) in zero dc field.

https://doi.org/10.1021/acs.inorgchem.1c00581
Inorg. Chem. 2021, 60, 8049−8061

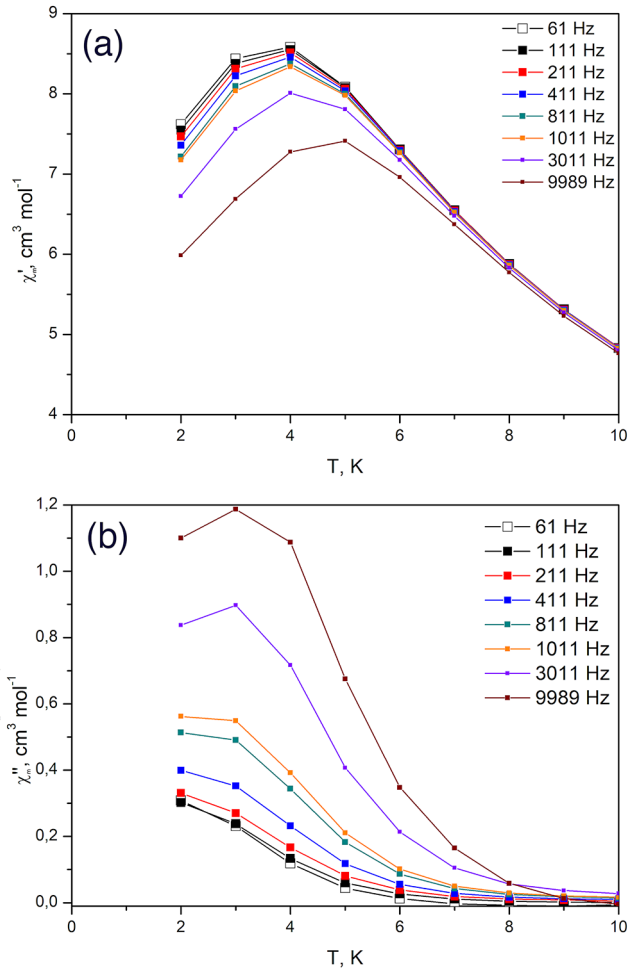

Figure 11. Temperature-dependent in-phase χ' (a) and out-of-phase χ'' (b) ac susceptibilities plots at different frequencies for $\mathbf{Dy_4}$ under an external dc field of 3000 Oe.

coordination polymer. The stability of the resulting ribbon structure, which is provided by H-bonds and the hydrophobic nature of the pivalate anions, allows one to obtain isostructural complexes for the majority of the lanthanide series both by aqueous and nonaqueous methods. This opens a prospect of creating mixed-metal complexes based on the $\mathbf{Ln_4}$ architecture for a fine-tuning of their properties. $\mathbf{Ln_4}$ hydroxo pivalates exist in two polymorphic forms (triclinic α-$\mathbf{Ln_4}$ and monoclinic β-$\mathbf{Ln_4}$) with a substantially different supramolecular arrangement of flattened ribbons and almost identical lattice energies. Dehydration of the as-obtained α-$\mathbf{Ln_4}$ polymorph leads to the loss of the translational symmetry along the ribbon and the formation of a hexagonal 2D-ordered $\mathbf{Ln_4}'$ mesostructure. Rehydration of $\mathbf{Ln_4}'$ surprisingly results in the restoration of 3D crystallinity, yielding the β-$\mathbf{Ln_4}$ phase. Despite the dramatic change in the ribbon arrangement, the local structure of the tetranuclear cluster remains intact through the two-step procedure. Although tetranuclear lanthanide compounds with a butterfly core are actively studied as potential single-molecule magnets, the $\mathbf{Ln_4}$ family is the first demonstration of a ribbon structure with tetranuclear units, which makes it possible to compare the single-molecule and single-chain magnetism in the lanthanide-pivalate system. Magnetic measurements reveal a weak antiferromagnetic coupling and slow magnetic relaxation in $\mathbf{Dy_4}$, $\mathbf{Dy_4}'$, $\mathbf{Ho_4}$, and $\mathbf{Er_4}$. Ab initio calculations reveal significant magnetic anisotropy of Ln^{3+} ions with an interplay between ferro- and antiferromagnetic interactions within tetranuclear $[Ln_4(OH)_2(piv)_{10}(H_2O)_2]$ species. At the same time, the data show that additional Ln···Ln interactions in the described $\mathbf{Ln_4}$ compounds compared to isolated tetranuclear clusters lead to enhancement of QTM which is suppressed under an external magnetic field, promoting the field-induced single-chain magnetic behavior of $\mathbf{Dy_4}$.

■ ASSOCIATED CONTENT

Supporting Information

The Supporting Information is available free of charge at https://pubs.acs.org/doi/10.1021/acs.inorgchem.1c00581.

MALDI and TGA data, characterization data on the compounds; unit cell parameters, interatomic distances, H-bond parameters, coordination polyhedra analysis, powder diffraction patterns, packing analysis; details on quantum chemical calculations; details on pair distribution function study; temperature-dependent magnetic susceptibility data, magnetization data, ac susceptibility data, angles of the main axes with molecular framework (PDF)

Accession Codes

CCDC 1984606−1984608 and 2025596−2025598 contain the supplementary crystallographic data for this paper. These data can be obtained free of charge via www.ccdc.cam.ac.uk/data_request/cif, or by emailing data_request@ccdc.cam.ac.uk, or by contacting The Cambridge Crystallographic Data Centre, 12 Union Road, Cambridge CB2 1EZ, UK; fax: +44 1223 336033.

■ AUTHOR INFORMATION

Corresponding Author

Dmitry Tsymbarenko − *Lomonosov Moscow State University, Moscow 119991, Russia;* orcid.org/0000-0002-2818-5639; Email: tsymbarenko@inorg.chem.msu.ru

Authors

Dimitry Grebenyuk − *Lomonosov Moscow State University, Moscow 119991, Russia;* orcid.org/0000-0002-4723-8564

Mirijam Zobel − *Chemistry Department, University Bayreuth, Bayreuth 95447, Germany;* orcid.org/0000-0002-8207-8316

Maurizio Polentarutti − *Elettra-Sincrotrone Trieste S.C.p.A, Basovizza, Trieste 34149, Italy*

Liviu Ungur − *Department of Chemistry, National University of Singapore, Singapore 117543, Singapore;* orcid.org/0000-0001-5015-4225

Mikhail Kendin − *Lomonosov Moscow State University, Moscow 119991, Russia;* orcid.org/0000-0003-2783-0023

Konstantin Zakharov − *Lomonosov Moscow State University, Moscow 119991, Russia*

Pavel Degtyarenko − *SuperOx, LLC, Moscow 117246, Russia; Joint Institute for High Temperature of the Russian Academy of Science, Moscow 125412, Russia*

Alexander Vasiliev − *Lomonosov Moscow State University, Moscow 119991, Russia; National University of Science and Technology "MISiS", Moscow 119049, Russia;* orcid.org/0000-0003-3558-6761

Complete contact information is available at:

https://doi.org/10.1021/acs.inorgchem.1c00581
Inorg. Chem. 2021, 60, 8049−8061

https://pubs.acs.org/10.1021/acs.inorgchem.1c00581

Author Contributions

D.T. conceived the idea, secured funding, and supervised the project. D.G., M.K., and D.T. synthesized and characterized the compounds. M.Z. enabled access to the lab diffractometer for PDF data collection, provided expertise in the field, and contributed to the data analysis and discussion. D.G. and D.T. performed DFT calculations. M.P. set up the single-crystal diffraction experiment at the beamline and assisted in data collection. D.G. and D.T. collected single-crystal and powder diffraction data, and solved and refined the crystal structures. K.Z. and P.D. performed dc and ac magnetic measurements; D.T. and D.G. interpreted the data. L.U. performed ab initio calculations, extracted the magnetic exchange constants, analyzed the obtained results and contributed to the respective section of the manuscript. A.V. supervised the magnetic measurements and contributed to the discussion. D.G. took the lead in writing of the manuscript with contributions from D.T., M.Z., and M.P. All authors have given approval to the final version of the manuscript.

Funding

D.T., D.G., and M.K. acknowledge the support by RSF (project No. 19-73-00277). M.Z. acknowledges funding by Deutsche Forschungsgemeinschaft (DFG, German Research Foundation) via SFB 840. A.V. acknowledges the support by the Megagrant 2020-220-08-6358 of the Government of the Russian Federation. Diffraction data collection at Elettra synchrotron was partially funded by the CALIPSOplus project from the EU Framework Programme for Research and Innovation HORIZON 2020 (Grant Agreement 730872). L.U. acknowledges the financial support of the research projects R-143-000-A65-133 and R-143-000-A80-114 of the National University of Singapore.

Notes

The authors declare no competing financial interest.

■ ACKNOWLEDGMENTS

D.T. and D.G. thank Jasper Plaisier and Giorgio Bais for their invaluable support during powder and single-crystal diffraction experiments. P.D. thanks S. Gavrilkin and A. Tsvetkov from the P. N. Lebedev Physical Institute of the Russian Academy of Sciences. The magnetic measurements were done at LPI Shared Facility Centre for Studies of HTS and other Strongly Correlated Materials in the P. N. Lebedev Physical Institute of the Russian Academy of Sciences. The research is carried out using the equipment of the shared research facilities of HPC computing resources at Lomonosov Moscow State University. Ab initio calculations of magnetism were done on the ASPIRE-1 cluster (www.nscc.sg) under the project 11001278. D.T., D.G., and M.K. acknowledge partial support from the M. V. Lomonosov Moscow State University Program of Development.

■ REFERENCES

(1) Sessoli, R.; Powell, A. K. Strategies towards Single Molecule Magnets Based on Lanthanide Ions. *Coord. Chem. Rev.* **2009**, *253* (19−20), 2328−2341.

(2) Abbas, G.; Lan, Y.; Kostakis, G. E.; Wernsdorfer, W.; Anson, C. E.; Powell, A. K. Series of Isostructural Planar Lanthanide Complexes $[Ln^{III}_4(\mu_3\text{-}OH)_2(mdeaH)_2(Piv)_8]$ with Single Molecule Magnet Behavior for the Dy4 Analogue. *Inorg. Chem.* **2010**, *49* (17), 8067−8072.

(3) Badiane, A. M.; Freslon, S.; Daiguebonne, C.; Suffren, Y.; Bernot, K.; Calvez, G.; Costuas, K.; Camara, M.; Guillou, O. Lanthanide-Based Coordination Polymers with a 4,5-Dichlorophthalate Ligand Exhibiting Highly Tunable Luminescence: Toward Luminescent Bar Codes. *Inorg. Chem.* **2018**, *57* (6), 3399−3410.

(4) Calvez, G.; Daiguebonne, C.; Guillou, O. Unprecedented Lanthanide-Containing Coordination Polymers Constructed from Hexanuclear Molecular Building Blocks: $\{[Ln_6O(OH)_8](NO_3)_2(bdc)(Hbdc)_2{\cdot}2NO_3{\cdot}H_2bdc\}_\infty$. *Inorg. Chem.* **2011**, *50* (7), 2851−2858.

(5) Ghiassi, K. B.; Olmstead, M. M.; Balch, A. L. Gadolinium-Containing Endohedral Fullerenes: Structures and Function as Magnetic Resonance Imaging (MRI) Agents. *J. Chem. Soc. Dalt. Trans.* **2014**, *43* (20), 7346−7358.

(6) Lammert, M.; Wharmby, M. T.; Smolders, S.; Bueken, B.; Lieb, A.; Lomachenko, K. A.; De Vos, D.; Stock, N. Cerium-Based Metal Organic Frameworks with UiO-66 Architecture: Synthesis, Properties and Redox Catalytic Activity. *Chem. Commun.* **2015**, *51* (63), 12578−12581.

(7) Pagis, C.; Ferbinteanu, M.; Rothenberg, G.; Tanase, S. Lanthanide-Based Metal Organic Frameworks: Synthetic Strategies and Catalytic Applications. *ACS Catal.* **2016**, *6* (9), 6063−6072.

(8) Park, J.; Pasupathy, A. N.; Goldsmith, J. I.; Chang, C.; Yaish, Y.; Petta, J. R.; Rinkoski, M.; Sethna, J. P.; Abruna, H. D.; McEuen, P. L.; Ralph, D. C. Coulomb Blockade and the Kondo Effect in Single-Atom Transistors. *Nature* **2002**, *417* (6890), 722−725.

(9) Fang, J.; You, H.; Chen, J.; Lin, J.; Ma, D. Memory Devices Based on Lanthanide (Sm^{3+}, Eu^{3+}, Gd^{3+}) Complexes. *Inorg. Chem.* **2006**, *45* (9), 3701−3704.

(10) Dinca, A. S.; Mindru, A.; Dragancea, D.; Tiseanu, C.; Shova, S.; Cornia, S.; Carrella, L. M.; Rentschler, E.; Affronte, M.; Andruh, M. Aggregation of [Ln III 12] Clusters by the Dianion of 3-Formylsalicylic Acid. Synthesis, Crystal Structures, Magnetic and Luminescence Properties. *Dalt. Trans.* **2019**, *48* (5), 1700−1708.

(11) Wang, W.-M.; Li, X.-Z.; Zhang, L.; Chen, J.-L.; Wang, J.-H.; Wu, Z.-L.; Cui, J.-Z. A Series of [2 × 2] Square Grid LnIII4 Clusters: A Large Magnetocaloric Effect and Single-Molecule-Magnet Behavior. *New J. Chem.* **2019**, *43*, 7419−7426.

(12) Guo, F. S.; Leng, J. D.; Liu, J. L.; Meng, Z. S.; Tong, M. L. Polynuclear and Polymeric Gadolinium Acetate Derivatives with Large Magnetocaloric Effect. *Inorg. Chem.* **2012**, *51* (1), 405−413.

(13) Yadav, M.; Mereacre, V.; Lebedkin, S.; Kappes, M. M.; Powell, A. K.; Roesky, P. W. Mononuclear and Tetranuclear Compounds of Yttrium and Dysprosium Ligated by a Salicylic Schiff-Base Derivative: Synthesis, Photoluminescence, and Magnetism. *Inorg. Chem.* **2015**, *54* (3), 773−781.

(14) Kuang, W. W.; Zhu, L. L.; Xu, Y.; Yang, P. P. A Tetranuclear Holmium Compound Exhibiting Single Molecule Magnet Behavior. *Inorg. Chem. Commun.* **2015**, *61*, 169−172.

(15) Langley, S. K.; Chilton, N. F.; Gass, I. A.; Moubaraki, B.; Murray, K. S. Planar Tetranuclear Lanthanide Clusters with the Dy4analogue Displaying Slow Magnetic Relaxation. *Dalt. Trans.* **2011**, *40* (47), 12656−12659.

(16) Bala, S.; Bishwas, M. S.; Pramanik, B.; Khanra, S.; Fromm, K. M.; Poddar, P.; Mondal, R. Construction of Polynuclear Lanthanide (Ln = DyIII, TbIII, and NdIII) Cage Complexes Using Pyridine-Pyrazole-Based Ligands: Versatile Molecular Topologies and SMM Behavior. *Inorg. Chem.* **2015**, *54* (17), 8197−8206.

(17) Guo, P. H.; Liu, J. L.; Jia, J. H.; Wang, J.; Guo, F. S.; Chen, Y. C.; Lin, W. Q.; Leng, J. D.; Bao, D. H.; Zhang, X. D.; Luo, J. H.; Tong, M. L. Multifunctional DyIII4 Cluster Exhibiting White-Emitting, Ferroelectric and Single-Molecule Magnet Behavior. *Chem. - Eur. J.* **2013**, *19* (27), 8769−8773.

(18) Wang, W. M.; Han, T. L.; Shao, Y. L.; Qiao, X. Y.; Wu, Z. L.; Wang, Q. L.; Shi, P. F.; Gao, H. L.; Cui, J. Z. Butterfly-Shaped Tetranuclear Ln4 Clusters Showing Magnetic Refrigeration and Single Molecule-Magnet Behavior. *New J. Chem.* **2018**, *42* (18), 14949−14955.

(19) Roitershtein, D. M.; Vinogradov, A. A.; Lyssenko, K. A.; Nifant'ev, I. E. Self-Assembly of Heteroleptic Tetranuclear Carboxylate Complexes of Yttrium and Lanthanides during Hydrolysis and Oxidation of Rare Earth Homoleptic Carboxylates. *Inorg. Chem. Commun.* **2017**, *84*, 225−228.
(20) Li, X.-Y.; Su, H.-F.; Li, Q.-W.; Feng, R.; Bai, H.-Y.; Chen, H.-Y.; Xu, J.; Bu, X.-H. A Giant Dy_{76} Cluster: A New Fused Bi-Nanopillar Structural Model in Lanthanide Clusters. *Angew. Chem., Int. Ed.* **2019**, *58*, 10184.
(21) Giester, G.; Žák, Z.; Unfried, P. Syntheses and Crystal Structures of Rare Earth Basic Nitrates Hydrates. Part III. $[Ln_6(\mu_6\text{-}O)(\mu_3\text{-}OH)_8(H_2O)_{12}(\eta^2\text{-}NO_3)_6](NO_3)_2{\cdot}xH_2O$, Ln = Y, Sm, Eu, Gd, Tb, Dy, Ho, Er, Tm, Yb, Lu; x = 3, 4, 5, 6. *J. Alloys Compd.* **2009**, *481* (1−2), 116−128.
(22) Žák, Z.; Unfried, P.; Giester, G. The Structures of Some Rare Earth Basic Nitrates $[Ln_6(\mu_6\text{-}O)(\mu_3\text{-}OH)_8(H_2O)_{12}(NO_3)_6](NO_3)_2{\cdot}xH_2O$, Ln=Y, Gd, Yb, x(Y, Yb)=4; x(Gd)=5. A Novel Rare Earth Metal Cluster of the M6X8 Type with Interstitial O Atom. *J. Alloys Compd.* **1994**, *205*, 235−242.
(23) Wang, R.; Liu, H.; Carducci, M. D.; Jin, T.; Zheng, C.; Zheng, Z. Lanthanide Coordination with α-Amino Acids under near Physiological PH Conditions: Polymetallic Complexes Containing the Cubane-like $[Ln_4(\mu_3\text{-}OH)_4]^{8+}$ Cluster Core. *Inorg. Chem.* **2001**, *40* (12), 2743−2750.
(24) Peng, J.-B.; Kong, X.-J.; Ren, Y.-P.; Long, L.-S.; Huang, R.-B.; Zheng, L.-S. Trigonal Bipyramidal Dy 5 Cluster Exhibiting Slow Magnetic Relaxation. *Inorg. Chem.* **2012**, *51* (4), 2186−2190.
(25) Wu, Z. L.; Dong, J.; Ni, W. Y.; Zhang, B. W.; Cui, J. Z.; Zhao, B. PH-Induced Dy4 and Dy10 Cluster-Based 1D Chains with Different Magnetic Relaxation Features. *Dalt. Trans.* **2014**, *43* (44), 16838−16845.
(26) Datta, S.; Baskar, V.; Li, H.; Roesky, P. W. Synthesis and Structural Characterization of Tetra- and Pentanuclear Lanthanide Hydroxido Clusters. *Eur. J. Inorg. Chem.* **2007**, *2007* (26), 4216−4220.
(27) Andrews, P. C.; Beck, T.; Forsyth, C. M.; Fraser, B. H.; Junk, P. C.; Massi, M.; Roesky, P. W. Templated Assembly of a $\mu_6\text{-}CO_3^{2-}$ Dodecanuclear Lanthanum Dibenzoylmethanide Hydroxido Cluster with Concomitant Formation of Phenylglyoxylate. *J. Chem. Soc. Dalt. Trans.* **2007**, *9226* (48), 5651−5654.
(28) Andrews, P. C.; Deacon, G. B.; Frank, R.; Fraser, B. H.; Junk, P. C.; MacLellan, J. G.; Massi, M.; Moubaraki, B.; Murray, K. S.; Silberstein, M. Formation of HoIII Trinuclear Clusters and GdIII Monodimensional Polymers Induced by Ortho and Para Regioisomers of Pyridyl-Functionalised â-Diketones: Synthesis, Structure, and Magnetic Properties. *Eur. J. Inorg. Chem.* **2009**, *2009* (6), 744−751.
(29) Grebenyuk, D.; Martynova, I.; Tsymbarenko, D. Self-Assembly of Hexanuclear Lanthanide Carboxylate Clusters of Three Architectures. *Eur. J. Inorg. Chem.* **2019**, *2019*, 3103−3111.
(30) Dybtsev, D. N.; Sapianik, A. A.; Fedin, V. P. Pre-Synthesized Secondary Building Units in the Rational Synthesis of Porous Coordination Polymers. *Mendeleev Commun.* **2017**, *27* (4), 321−331.
(31) Mahé, N.; Guillou, O.; Daiguebonne, C.; Gérault, Y.; Caneschi, A.; Sangregorio, C.; Chane-Ching, J. Y.; Car, P. E.; Roisnel, T. Polynuclear Lanthanide Hydroxo Complexes: New Chemical Precursors for Coordination Polymers. *Inorg. Chem.* **2005**, *44* (22), 7743−7750.
(32) Li, J. R.; Kuppler, R. J.; Zhou, H. C. Selective Gas Adsorption and Separation in Metal-Organic Frameworks. *Chem. Soc. Rev.* **2009**, *38* (5), 1477−1504.
(33) Hu, F.; Di, Z.; Wu, M.; Hong, M.; Li, J. A Robust Multifunctional Eu6-Cluster Based Framework for Gas Separation and Recognition of Small Molecules and Heavy Metal Ions. *Cryst. Growth Des.* **2019**, *19* (11), 6381−6387.
(34) Diamantis, S. A.; Margariti, A.; Pournara, A. D.; Papaefstathiou, G. S.; Manos, M. J.; Lazarides, T. Luminescent Metal-Organic Frameworks as Chemical Sensors: Common Pitfalls and Proposed Best Practices. *Inorg. Chem. Front.* **2018**, *5* (7), 1493−1511.
(35) Zhao, S. N.; Wang, G.; Poelman, D.; Van Der Voort, P. Luminescent Lanthanide MOFs: A Unique Platform for Chemical Sensing. *Materials* **2018**, *11* (4), 572.
(36) Bo, Q. B.; Zhang, H. T.; Wang, H. Y.; Miao, J. L.; Zhang, Z. W. Anhydrous Lanthanide MOFs and Direct Photoluminescent Sensing for Polyoxometalates in Aqueous Solution. *Chem. - Eur. J.* **2014**, *20* (13), 3712−3723.
(37) Kundu, T.; Mitra, S.; Patra, P.; Goswami, A.; Díazdíaz, D.; Banerjee, R. Mechanical Downsizing of a Gadolinium(III)-Based Metal-Organic Framework for Anticancer Drug Delivery. *Chem. - Eur. J.* **2014**, *20* (33), 10514−10518.
(38) Wu, Y.; Morton, S.; Kong, X.; Nichol, G. S.; Zheng, Z. Hydrolytic Synthesis and Structural Characterization of Lanthanide-Acetylacetonato/Hydroxo Cluster Complexes-A Systematic Study. *Dalt. Trans.* **2011**, *40* (5), 1041−1046.
(39) Ke, H.; Gamez, P.; Zhao, L.; Xu, G. F.; Xue, S.; Tang, J. Magnetic Properties of Dysprosium Cubanes Dictated by the M-O-M Angles of the $[Dy_4(\mu_3\text{-}OH)_4]$ Core. *Inorg. Chem.* **2010**, *49* (16), 7549−7557.
(40) Baril-Robert, F.; Petit, S.; Pilet, G.; Chastanet, G.; Reber, C.; Luneau, D. Site-Selective Lanthanide Doping in a Nonanuclear Yttrium(III) Cluster Revealed by Crystal Structures and Luminescence Spectra. *Inorg. Chem.* **2010**, *49* (23), 10970−10976.
(41) Li, X. L.; He, L. F.; Feng, X. L.; Song, Y.; Hu, M.; Han, L. F.; Zheng, X. J.; Zhang, Z. H.; Fang, S. M. Two Chiral Tetradecanuclear Hydroxo-Lanthanide Clusters with Luminescent and Magnetic Properties. *CrystEngComm* **2011**, *13* (11), 3643−3645.
(42) Yi, X.; Bernot, K.; Calvez, G.; Daiguebonne, C.; Guillou, O. 3D Organization of Dysprosium Cubanes. *Eur. J. Inorg. Chem.* **2013**, *2013* (34), 5879−5885.
(43) Savard, D.; Lin, P. H.; Burchell, T. J.; Korobkov, I.; Wernsdorfer, W.; Clérac, R.; Murugesu, M. Two-Dimensional Networks of Lanthanide Cubane-Shaped Dumbbells. *Inorg. Chem.* **2009**, *48* (24), 11748−11754.
(44) Biswas, S.; Mondal, A. K.; Konar, S. Densely Packed Lanthanide Cubane Based 3D Metal-Organic Frameworks for Efficient Magnetic Refrigeration and Slow Magnetic Relaxation. *Inorg. Chem.* **2016**, *55* (5), 2085−2090.
(45) Xue, D. X.; Belmabkhout, Y.; Shekhah, O.; Jiang, H.; Adil, K.; Cairns, A. J.; Eddaoudi, M. Tunable Rare Earth Fcu-MOF Platform: Access to Adsorption Kinetics Driven Gas/Vapor Separations via Pore Size Contraction. *J. Am. Chem. Soc.* **2015**, *137* (15), 5034−5040.
(46) Angeli, G. K.; Sartsidou, C.; Vlachaki, S.; Spanopoulos, I.; Tsangarakis, C.; Kourtellaris, A.; Klontzas, E.; Froudakis, G. E.; Tasiopoulos, A.; Trikalitis, P. N. Reticular Chemistry and the Discovery of a New Family of Rare Earth (4, 8)-Connected Metal-Organic Frameworks with Csq Topology Based on $RE_4(\mu_3\text{-}O)_2(COO)_8$ Clusters. *ACS Appl. Mater. Interfaces* **2017**, *9* (51), 44560−44566.
(47) Liu, S. J.; Zhao, J. P.; Song, W. C.; Han, S. De; Liu, Z. Y.; Bu, X. H. Slow Magnetic Relaxation in Two New 1D/0D DyIII Complexes with a Sterically Hindered Carboxylate Ligand. *Inorg. Chem.* **2013**, *52* (4), 2103−2109.
(48) Tsymbarenko, D.; Martynova, I.; Grebenyuk, D.; Shegolev, V.; Kuzmina, N. One-Dimensional Coordination Polymers of Whole Row Rare Earth Tris-Pivalates. *J. Solid State Chem.* **2018**, *258*, 876−884.
(49) Tsymbarenko, D. M.; Martynova, I. A.; Malkerova, I. P.; Alikhanyan, A. S.; Kuzmina, N. P. Mixed Ligand Acetate, Propionate, and Pivalate Complexes of Rare Earth Metals with Monoethanolamine: A New Approach to the Synthesis, Composition, Structure, and Use for the Preparation of Oxide Materials. *Russ. J. Coord. Chem.* **2016**, *42* (10), 662−678.
(50) Torres, S. G.; Meyer, G. Anhydrous Neodymium(III) Acetate. *Z. Anorg. Allg. Chem.* **2008**, *634* (2), 231−233.
(51) Lossin, A.; Meyer, G. $Pr(CH_3COO)_3$, Ein Wasserfreies Selten-Erd-Acetat Mit Netzwerkstruktur. *Z. Anorg. Allg. Chem.* **1994**, *620*, 438−443.

https://doi.org/10.1021/acs.inorgchem.1c00581
Inorg. Chem. 2021, 60, 8049−8061

(52) Meyer, G.; Gieseke-Vollmer, D. Das Wasserfreie Lanthanacetat, $La(CH_3COO)_3$, and Sein Precursor, $(NH_4)_3[La(CH_3COO)_6]$ 1/ $2H_2O$. *Z. Anorg. Allg. Chem.* **1993**, *619*, 1603−1608.
(53) Torres, S. G.; Pantenburg, I.; Meyer, G. Direct Oxidation of Europium Metal with Acetic Acid: Anhydrous Europium(III) Acetate, $Eu(OAc)_3$, Its Sesqui-Hydrate, $Eu(OAc)_3(H_2O)_{1.5}$, and the " Hydrogendiacetate", $[Eu(H(OAc)_2)_3](H_2O)$. *Z. Anorg. Allg. Chem.* **2006**, *632* (12−13), 1989−1994.
(54) Lossin, A.; Meyer, G. $Cs_2(H_3O)Pr(CH_3COO)_6$ Und $Cs_2Pr(CH_3COO)_5$: Synthese, Kristallstrukturen Und Thermolyse. Uber Die Analogen Acetate Mit Lanthan Bis Terbium. *Z. Anorg. Allg. Chem.* **1993**, *619*, 2021−2030.
(55) Zhang, K.; Montigaud, V.; Cador, O.; Li, G. P.; Le Guennic, B.; Tang, J. K.; Wang, Y. Y. Tuning the Magnetic Interactions in Dy(III)4 Single-Molecule Magnets. *Inorg. Chem.* **2018**, *57* (14), 8550−8557.
(56) Zhang, K.; Li, G. P.; Zhang, C.; Wang, Y. Y. Tetranuclear Dysprosium Compound: Synthesis and Single-Molecule Magnet Properties. *J. Solid State Chem.* **2019**, *273*, 11−16.
(57) Casanova, D.; Llunell, M.; Alemany, P.; Alvarez, S. The Rich Stereochemistry of Eight-Vertex Polyhedra: A Continuous Shape Measures Study. *Chem. - Eur. J.* **2005**, *11* (5), 1479−1494.
(58) Terban, M. W.; Shi, C.; Silbernagel, R.; Clearfield, A.; Billinge, S. J. L. Local Environment of Terbium(III) Ions in Layered Nanocrystalline Zirconium(IV) Phosphonate-Phosphate Ion Exchange Materials. *Inorg. Chem.* **2017**, *56* (15), 8837−8846.
(59) Thomä, S. L. J.; Krauss, S. W.; Eckardt, M.; Chater, P.; Zobel, M. Atomic Insight into Hydration Shells around Facetted Nanoparticles. *Nat. Commun.* **2019**, *10* (1), 1−7.
(60) Ungur, L.; Leroy, J. J.; Korobkov, I.; Murugesu, M.; Chibotaru, L. F. Fine-Tuning the Local Symmetry to Attain Record Blocking Temperature and Magnetic Remanence in a Single-Ion Magnet. *Angew. Chem., Int. Ed.* **2014**, *53* (17), 4413−4417.
(61) Guo, P. H.; Liu, J. L.; Zhang, Z. M.; Ungur, L.; Chibotaru, L. F.; Leng, J. D.; Guo, F. S.; Tong, M. L. The First {Dy 4} Single-Molecule Magnet with a Toroidal Magnetic Moment in the Ground State. *Inorg. Chem.* **2012**, *51* (3), 1233−1235.
(62) Anwar, M. U.; Al-Harrasi, A.; Rawson, J. M.; Gavey, E. L.; Regier, J.; Alexandropoulos, D.; Pilkington, M.; Thompson, L. K. Slow Magnetic Relaxation in Dy2 and Dy4 Complexes of a Versatile, Trifunctional Polydentate N,O-Ligand. *Dalton Trans.* **2019**, *48* (38), 14269−14278.
(63) Han, L. J.; Chen, J.; Zhang, Z. Q.; Zhang, H. H.; Kang, T. T.; Wang, W. M.; Mu, S. L.; Shi, Y. Synthesis, Structure and Slow Magnetic Relaxation of a Linear Ho4 Cluster. *Inorg. Chem. Commun.* **2018**, *96*, 52−55.
(64) Zhang, Y. X.; Li, M.; Liu, B. Y.; Wu, Z. L.; Wei, H. Y.; Wang, W. M. A Series of Planar Tetranuclear Lanthanide Complexes: Axial Ligand Modulated Magnetic Dynamics in Dy4 Species. *RSC Adv.* **2017**, *7* (87), 55523−55535.
(65) Lan, Y.; Klyatskaya, S.; Ruben, M.; Fuhr, O.; Wernsdorfer, W.; Candini, A.; Corradini, V.; Lodi Rizzini, A.; Del Pennino, U.; Troiani, F.; Joly, L.; Klar, D.; Wende, H.; Affronte, M. Magnetic Interplay between Two Different Lanthanides in a Tris-Phthalocyaninato Complex: A Viable Synthetic Route and Detailed Investigation in the Bulk and on the Surface. *J. Mater. Chem. C* **2015**, *3* (38), 9794−9801.
(66) Tang, J.; Hewitt, I.; Madhu, N. T.; Chastanet, G.; Wernsdorfer, W.; Anson, C. E.; Benelli, C.; Sessoli, R.; Powell, A. K. Dysprosium Triangles Showing Single-Molecule Magnet Behavior of Thermally Excited Spin States. *Angew. Chem.* **2006**, *118* (11), 1761−1765.
(67) Chibotaru, L. F.; Ungur, L.; Soncini, A. The Origin of Nonmagnetic Kramers Doublets in the Ground State of Dysprosium Triangles: Evidence for a Toroidal Magnetic Moment. *Angew. Chem.* **2008**, *120* (22), 4194−4197.
(68) Bartolomé, J.; Filoti, G.; Kuncser, V.; Schinteie, G.; Mereacre, V.; Anson, C. E.; Powell, A. K.; Prodius, D.; Turta, C. Magneto-structural Correlations in the Tetranuclear Series of $\{Fe_3LnO_2\}$ Butterfly Core Clusters: Magnetic and Mössbauer Spectroscopic Study. *Phys. Rev. B: Condens. Matter Mater. Phys.* **2009**, *80* (1), 1−16.
(69) Brunet, G.; Habib, F.; Korobkov, I.; Murugesu, M. Slow Magnetic Relaxation Observed in Dysprosium Compounds Containing Unsupported Near-Linear Hydroxo- and Fluoro-Bridges. *Inorg. Chem.* **2015**, *54* (13), 6195−6202.

https://doi.org/10.1021/acs.inorgchem.1c00581
Inorg. Chem. 2021, 60, 8049−8061